Far-infrared photodetectors based on graphene/black-AsP heterostructures

doi: 10.1364/OE.376299

Research Article | Vol. 28, No. 2 / 20 January 2020 / Optics Express 2480
Optics EXPRESS

Far-infrared photodetectors based on graphene/black-AsP heterostructures

VICTOR RYZHII,[1,2,3,*] MAXIM RYZHII,[4] VLADIMIR MITIN,[5] MICHAEL S. SHUR,[6] AND TAIICHI OTSUJI[1]

[1]Research Institute of Electrical Communication, Tohoku University, Sendai 980-8577, Japan
[2]Institute of Ultra High Frequency Semiconductor Electronics of RAS, Moscow 117105, Russia
[3]Center of Photonics and Two-Dimensional Materials, Moscow Institute of Physics and Technology, Dolgoprudny 141700, Russia
[4]Department of Computer Science and Engineering, University of Aizu, Aizu-Wakamatsu 965-8580, Japan
[5]Department of Electrical Engineering, University at Buffalo, Buffalo, NY 14228, USA
[6]Department of Electrical, Computer, and Systems Engineering and Department of Physics, Applied Physics, and Astronomy, Rensselaer Polytechnic Institute, Troy, New York 12180, USA
*v-ryzhii@riec.tohoku.ac.jp

Abstract: We develop the device models for the far-infrared interband photodetectors (IPs) with the graphene-layer (GL) sensitive elements and the black Phosphorus (b-P) or black-Arsenic (b-As) barrier layers (BLs). These far-infrared GL/BL-based IPs (GBIPs) can operate at the photon energies $\hbar\Omega$ smaller than the energy gap, Δ_G, of the b-P or b-As or their compounds, namely, at $\hbar\Omega \lesssim 2\Delta_G/3$ corresponding to the wavelength range $\lambda \gtrsim (6-12)$ μm. The GBIP operation spectrum can be shifted to the terahertz range by increasing the bias voltage. The BLs made of the compounds b-As_xB_{1-x} with different x, enable the GBIPs with desirable spectral characteristics. The GL doping level substantially affects the GBIP characteristics and is important for their optimization. A remarkable feature of the GBIPs under consideration is a substantial (over an order of magnitude) lowering of the dark current due to a partial suppression of the dark-current gain accompanied by a fairly high photoconductive gain. Due to a large absorption coefficient and photoconductive gain, the GBIPs can exhibit large values of the internal responsivity and dark-current-limited detectivity exceeding those of the quantum-well and quantum-dot IPs using the intersubband transitions. The GBIPs with the b-P and b-As BLs can operate at longer radiation wavelengths than the infrared GL-based IPs comprising the BLs made of other van der Waals materials and can also compete with all kinds of the far-infrared photodetectors.

1. Introduction

The terahertz (THz), far-infrared (FIR), and mid-infrared (MIR) photodetectors with elevated characteristics have found numerous applications [1–4]. The gapless energy spectrum of the graphene layers (GLs) [5] enables the possibility using the interband transitions in the GLs for the detection of normally incident electromagnetic radiation in a wide spectral range, including the THz, FIR, and MIR ranges (see, for example, [6–11]) .

The emergence of the black-Phosphorus (b-P), black-Arsenic (b-As), and the compounds of these materials (b-As_xP_{1-x}), in which the energy gap Δ_G varies from 0.15 to 1.2 eV, opens new prospects for the creation of the FIR and MIR photodetectors [12–21]. The combination of the GLs with the b-As_xP_{1-x} few-atomic layers and relatively thick barrier layers (BLs) can be useful for the enhancement of FIR/MIR interband photodetectors (IPs) performance.

Previously, we proposed and evaluated the vertical infrared GL-based IPs (GBIPs), in which the GLs are separated by the BLs made of van der Waals materials [22–25]. These GBIPs comprise the n-type emitter (thermionic or tunneling) and a single or multiple GLs with the

#376299 https://doi.org/10.1364/OE.376299
Journal © 2020 Received 28 Aug 2019; revised 8 Nov 2019; accepted 30 Nov 2019; published 17 Jan 2020

Optics EXPRESS

band alignment of the BLs and GL corresponding to the energy barrier for the electrons in the GL (counted from the Dirac point) Δ_C markedly smaller that for the holes Δ_V [26]. Their operation is associated with the interband electron photoexcitation by the photons with the energy $\hbar\Omega/2 \gtrsim \Delta_C$ (but $\hbar\Omega<\Delta_V$) to the states above the BL conductive band edge ($\hbar$ is the reduced Planck constant and Ω is the circular photon frequency). The photoexcited electrons contribute to the terminal photocurrent. The charge of the thermally generated and photogenerated but trapped holes controls the potential distribution across the photodetector structure and causes the injection of extra electrons from the n-emitter. The latter enables the dark-current and photoconductive gain. The gain which can be large providing a low probability of the electron capture to the GL (or GLs). The IPs exploiting a similar operation principle can be based on the GL/b-As_xP_{1-x}/GL heterostructures with the bulk BLs (comprising multiple-atomic sheets) exhibiting fairly narrow energy gaps [27–31] and, hence, smaller barrier energies Δ_C and Δ_V. However, in such heterostructures, $\Delta_V<\Delta_C$ [27]. Hence the hole photoescape from the GL is crucial (when $2\Delta_V \lesssim \hbar\Omega<2\Delta_C$). The hole photoescape from the GL into the BLs and then to the contact, can be the main operation mechanism. Due to this, the IPs based on the GL-based heterostructures with the b-As_xP_{1-x} BLs (GBIPs) can detect even longer wavelength radiation than the bulk IPs using the interband transitions in b-As_xP_{1-x} absorbing layers [15–19]. Indeed, the detectors with b-P and b-As absorbing bulk layers can be used at $\hbar\Omega>\Delta_G = \Delta_C + \Delta_V>0.30$ eV and $\hbar\Omega>0.15$ eV, respectively (that corresponds to the wavelengths $\lambda<8\mu$m and $\lambda<4\mu$m). However the GBIPs can detect the radiation with $\hbar\Omega \lesssim 0.2$ eV (b-P BLs, $\lambda \gtrsim 6\mu$m) and $\hbar\Omega \lesssim 0.1$ eV (b-As BLs, $\lambda \gtrsim 12\mu$m), i.e., can operate in the FIR radiation range. The black-Phosphorus Carbide (b-PC) BLs having fairly narrow energy gap can also be (for example, see [32,33]) used in the GBIPs operating in the range $\hbar\Omega<\Delta_G \sim 0.15$ eV.

In this paper, we consider the FIR GBIPs based on b-P/GL and b-As/GL heterostructures with a single GL playing the role of the photosensitive element (GL-base) and evaluate their performance accounting the specific features of these devices:

(i) Due to $\Delta_C>\Delta_V$ [27], we focus on the GBIP operation associated with the hole photoescape from the GL-base, that corresponds to the spectral range $2\Delta_V \lesssim \hbar\Omega<\Delta_G$;

(ii) Since, in the GBIPs with $\Delta_V<\Delta_C$ the holes play the major role, we consider the GBIPs based on b-P/GL and b-As/GL heterostructures supplied by the p-type contacts;

(iii) Because of a moderate value of Δ_C (being in the materials under consideration only somewhat larger than Δ_V), the thermal escape of the electrons from the GL-base into the BL conduction bands, affects the GBIP characteristics.

As demonstrated using the developed device model, the GBIPs under consideration can exhibit nontrivial features. These features enable a significant reduction of the dark-current gain (noise gain) combined with an elevated photoconductive gain. This is because of the contribution of the electron thermionic emission from the GL-base affecting the GL-base charge balance. Relatively high values of the photoconductive gain and of the interband absorption coefficient lead to the enhanced GBIP responsivity. The fact that the photoconductive gain can exceed the dark-current gain is beneficial for the realization of higher values of the GBIP dark-current-limited detectivity. Due to the relatively low energies of the hole interband photoescape, GBIPs can be very effective in the wavelength range $\lambda \gtrsim (6-12)\mu$m and longer at elevated temperatures. At sufficiently high electric fields in the BLs, the hole photoescape from the GL-base can be efficient even at $\hbar\Omega<\Delta_V/2$. This might extend the GBIP operation toward the THz spectral range. The optimized GBIPs can substantially surpass the quantum-well and quantum-dot IPs QWIPs and QDIPs) and compete with other FIR photodetectors, particularly at elevated temperatures.

The paper is organized as follows. After the introduction, in Sec. 2, we consider the GBIP device model and write down the pertinent model equations. In Sec. 3, we derive the general equations governing the terminal current in the GBIPs accounting for the carrier (hole and electron) thermionic emission, the hole photoescape due to the interband absorption of FIR

Optics EXPRESS

photons, and the capture of the carriers propagating in the BLs into the GL. Section 4 deals with the derivation of the dark-current gain and dark current-voltage characteristics and their analysis. In Secs. 5 and 6, the photocurrent, the GBIP detector responsivity, and the dark-current-limited detectivity are calculated using the results of Secs. 3 and 4. In Secs. 7 and 8, we discuss the model limitations and draw the main conclusions. Supplementary calculations are presented in Appendices A and B.

2. GBIP device model

We limit our analysis to the GBIPs with a single floating n-type GL-base separated by the undoped bulk b-P or b-As BLs supplied with p^+-type GLs serving as the emitter and the collector. The GBIPs with a single n-type GL-base with bulk p^+ contacts (one of which can be the substrate) exhibit similar properties. Thus the GBIPs under consideration constitute the p^+-GL/i-BL/n-GL/i-B/p^+-GL (or p^+-GL/i-BL/n-GL/i-BL/p^+-substrate) heterostructure. Such a GBIP is actually the phototransistor with the floating GL-base and with the GL-emitter and collector. The bias voltage V is applied between the emitter and the collector. For the definiteness and obtaining less cumbersome formulas, we focus on the GBIP having a virtually symmetric structure. In the GBIPs, the GL Dirac point stays within the gap of the BLs with $\Delta_V<\Delta_C$ [27]. The GBIP is illuminated by the incident FIR radiation with the photon energy in the range $2\Delta_V \lesssim \hbar\Omega<\Delta_G = \Delta_V + \Delta_C<2\Delta_C$. The operation of similar IPs in a shorter wavelength spectral range $\hbar\Omega>\Delta_G$, which corresponds to the interband absorption not only in the GL-base but also in the BLs, is beyond our consideration.

Figure 1 shows the GBIP band diagrams at moderate and relatively high forward bias voltages V and demonstrate the main hole and electron processes responsible for the GBIP operation. The potentials of the emitter and collector contacts in the GBIP are set $\varphi_E = 0$ (at $x = 0$) and $\varphi_C = -V$ (at $x = 2d$), respectively. Here d is the thickness of the BLs (assumed to be the same for both BLs), and axis x is directed perpendicular to the GBIP layers. The effective GBIP operation requires a sufficiently strong bias: $V \gg k_BT/e$, where $e = |e|$ is the value of the electron charge and k_B and T are the Boltzmann constant and the temperature.

Depending on the bias voltage, the electric field, E_E, in the emitter BL (EBL) adjacent to the emitter contacts can be both negative (at moderate voltages) and positive (at sufficiently high voltages). The electric field, E_C, in the collector BL (CBL) at the bias voltages under consideration is positive. The latter provides the effective removal of at least a part of the thermogenerated and photoexcited holes from the GL and their transport to the collector contacts (see Fig. 1).

In the GBIPs with a single GL-base, the emitter contact plays an important role. This is in contrast to the various multiple-GL devices [22–25] and the multiple QWIPs [2,34,35] studied previously, the emitter is able to supply a sufficient number of carriers to maintain the carrier balance in the GL (in the QWs of the QWIP). Therefore, the model needs to account for the carrier injection from the emitter. The densities of the hole current, injected from the p-type EGL and CGL can be generally presented as a functions of the acceptor density Σ_A and of the electric fields, E_E and E_C, at the interfaces between the EGL and the GL-base and between the GL-base and the CBL. We assume that in the heterostructures in question with the energy barriers Δ_C and Δ_V at the operation temperatures (see below), the quasi-equilibrium holes and electrons residing in the GLs can leave the latter primarily due to the thermionic emission via the barriers of the height Δ_V and Δ_C, respectively. Due to this, we assume the injection from the contact is of the thermionic origin with the rates, $\Theta_{E,p}$, $\Theta_{C,p}$, Θ_{E_n}, and Θ_{C_n}, of the hole and electron thermionic emission from the EGL and CGL given by (similar to that in [36])

$$\Theta_{E,p} = \frac{\Sigma_{GL}}{\tau_{esc}} \exp\left(\frac{\mu_E - \Delta_V}{k_BT}\right), \qquad \Theta_{C,p} = \frac{\Sigma_{GL}}{\tau_{esc}} \exp\left(\frac{\mu_C - \Delta_V}{k_BT}\right), \tag{1}$$

Optics EXPRESS

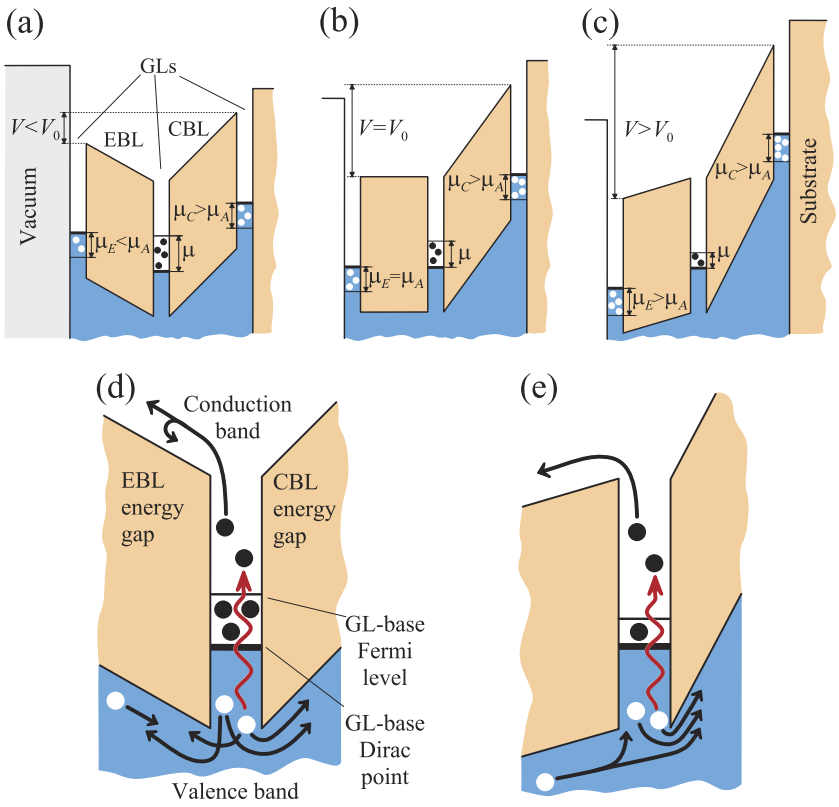

Fig. 1. The GBIP band diagrams (a) at relatively small ($V<V_0$), (b) $V = V_0$, and (c) high ($V>V_0$) bias voltages. Panels (d) and (e) show enlarged fragments of the device band diagrams demonstrating the processes of the holes (black circles) an electrons (open circles) transitions indicated by arrows. The wavy vertical arrow shows the electron transfer from the valence band in the GL to its conduction band due to the photon absorption.

$$\Theta_{E,n} = \frac{\Sigma_{GL}}{\tau_{esc}} \exp\left(-\frac{\mu_E + \Delta_C}{k_B T}\right) \qquad \Theta_{C,n} = \frac{\Sigma_{GL}}{\tau_{esc}} \exp\left(-\frac{\mu_C + \Delta_C}{k_B T}\right), \tag{2}$$

Here Σ_{GL} is the characteristic carrier density in the GL, τ_{esc} is the characteristic time of the carrier escape from the GL (try-to-escape time), μ_E and μ_C are the hole Fermi energy in the emitter and collector GLs determined by the acceptor density Σ_A and the density of the holes induced by the electric field in the EBL and CBL E_E and E_C , respectively.

Due to the degeneracy of the hole gas in the heavily doped emitter GL, the quantities μ_E and μ_C are

$$\mu_E = \sqrt{\mu_A^2 + \frac{\kappa\hbar^2 v_W^2 E_E}{4e}} \simeq \mu_A\left(1 + \frac{eE_E d}{2eV_A}\right), \qquad \mu_C = \sqrt{\mu_A^2 - \frac{\kappa\hbar^2 v_W^2 E_C}{4e}} \simeq \mu_A\left(1 + \frac{eE_C d}{2eV_A}\right), \tag{3}$$

where κ is the dielectric constant of the BL material, $\mu_A \simeq \hbar v_W \sqrt{\pi\Sigma_A}$, $V_A = 4\pi ed\Sigma_A/\kappa$, and $v_W \simeq 10^8$ cm/s is the characteristic carrier velocity in GLs.

The hole and electron thermionic fluxes, Θ_p and Θ_n, from the GL-base to the contacts can be presented as

$$\Theta_p = \frac{\Sigma_{GL}}{\tau_{esc}} \exp\left(-\frac{\mu + \Delta_V}{k_B T}\right), \qquad \Theta_n = \frac{\Sigma_{GL}}{\tau_{esc}} \exp\left(\frac{\mu - \Delta_C}{k_B T}\right), \tag{4}$$

Optics EXPRESS

where μ is the Fermi energy of the electron-hole system in the GL (counted from the Dirac point). When the electron density, Σ, in the GL exceeds the donor density Σ_D, $\mu>0$.

In the spectral range under consideration, the interband radiation absorption leads to the photoescape of the holes from the GL-base either directly (if $\hbar\Omega \geq 2\Delta_V$ or via tunneling following the hole photoexcitation (if $\hbar\Omega \lesssim 2\Delta_V$) with the rate G_{ph}, of the photoescape from the GL-base, given by

$$G_{ph} = \beta F_\Omega \xi_\Omega I_\Omega. \tag{5}$$

Here $\beta = (\pi e^2/\hbar c\sqrt{\kappa_{BL}}) \simeq 0.023/\sqrt{\kappa_{BL}}$ is the GL interband absorption coefficient, $\sqrt{\kappa_{BL}}$ is the barrier material refractive index, I_Ω is the intensity of radiation incident on the GL at its plane (the flux of the incident photons), c is the speed of light in vacuum, The factor F_Ω is associated with the Pauli principle and is given by

$$F_\Omega = \frac{1}{\exp[(\mu - \hbar\Omega/2)/k_BT] + 1}. \tag{6}$$

For the escape probabilities of the photoexcited holes from the GL-base we use the following simplified formula accounting for the possibility of tunneling through the triangular barriers formed by the pertinent electric fields [22,23]:

$\xi_\Omega = (1 + \tau_{esc}/\tau_{relax})^{-1}$ when $\hbar\Omega \geq 2\Delta_V$, and

$$\frac{1}{\xi_\Omega} = 1 + \frac{\tau_{esc}}{\tau_{relax}}\left\{\exp\left[\frac{4\sqrt{2m_z}(\Delta_V - \hbar\Omega/2)^{3/2}}{3e\hbar E_E\theta(-E_E)}\right] + \exp\left[\frac{4\sqrt{2m_z}(\Delta_V - \hbar\Omega/2)^{3/2}}{3e\hbar E_C\theta(E_C)}\right]\right\}, \tag{7}$$

when $\hbar\Omega \leq 2\Delta_V/2$. Here τ_{relax} is the energy relaxation time of the photoexcited holes, m_z is the carrier effective mass in the BLs in the direction perpendicular to the atomic sheets and $\theta(z) = 1$ for $z \geq 0$ and $\theta(z) = 0$ for $z<0$ is the Heaviside step-unity function.

The carrier Fermi energy in the GL-base μ and the density of the net current across the device heterostructure j can be found as function of the structural parameter, carrier temperature, applied bias voltage V, and the incident radiation intensity I_Ω considering the balance of the carrier emission from and their capture into the GL-base.

To describe the balance of the carrier emitted from the GL-base and captured into it, we assume that the carrier capture rate is proportional to the probability, p, of the capture of the carrier crossing the GL-base. The concept of the capture probability, introduced in Ref. [37], was widely used in the models of the QW and GL devices [22–25,30,31,34–36,38–40]. The capture probability p strongly dependent on the energy of the carriers crossing the GL (or QW) and, hence on the electric fields around the GL [35,36,38,41,42]. However, in the situations when E_E is small, i.e., when $V \lesssim V_0$ corresponding to Figs. 1(a) and 1(b), one can set $p = const$. Normally, $p \ll 1$ [38,39].

The balance equation should be supplemented by an equation relating E_E and E_C ($E_E + E_C = V/d$) with the GL-base charge density $e\Sigma$ (the Poisson equation): $E_C - E_E = (4\pi e/\kappa)(\Sigma_D - \Sigma)$. Considering that $E_E + E_C = (eV + \mu_C - \mu_E)/ed \simeq V - \mu_A(E_E + E_C)/2dE_A$ and expressing Σ via the Fermi energy μ (see Appendix A), we obtain

$$V^* - V_D - V_T\left[\mathcal{F}_1\left(-\frac{\mu}{k_BT}\right) - \mathcal{F}_1\left(\frac{\mu}{k_BT}\right)\right] = 2E_Ed. \tag{8}$$

Here $V^* = V/(1 + \mu_A/2eV_A)$, $V_D = (4\pi edN_D/\kappa)$, $V_T = (8edk_B^2T^2/\kappa\hbar^2v_W^2)$, and $\mathcal{F}_1(a)$ is the Fermi-Dirac integral [43,44]:

$$\mathcal{F}_1(a) = \int_0^\infty \frac{d\xi\xi}{\exp(\xi - a) + 1}.$$

A distinction between V^* and V is due to the quantum capacitance [45] in the heterostructure under consideration. Since at the practical values of the GBIP structural parameters, the quantity

Optics EXPRESS

μ_A/eV_A in the expression for V^* is very small, in the following we disregard the effect of quantum capacitance and, hence, neglect the above distinction.

As seen from Fig. 1, the GBIP band diagram depends on the bias voltage V. At relatively low bias voltages $V<V_0$, where V_0 is a certain threshold voltage determined in the following, the electric fields in the emitter and collector BLs, E_E and E_C, are respectively negative and positive: $E_E<0$ and $E_C>0$. At $V = V_0$, $E_E = 0$, while at $V>V_0$ both E_E and E_C are positive. In the following, we restrict our treatment by the GBIP operation at moderate bias voltages ($V \le V_0$), where it is most effective.

3. Dark current and photocurrent densities

Considering Eqs. (1) - (7), for $\mu_E = \mu_C = \mu_A$ the equation governing the equality of the carrier fluxes into and out of the GL-base can be presented as

$$\frac{j_{GL}}{e}\exp\left(-\frac{\Delta_G}{2k_BT}\right)\left[\exp\left(\frac{\mu_0+\mu_A}{k_BT}\right)\exp\left(\frac{eE_Ed}{k_BT}\right)+\exp\left(\frac{\mu_0+\mu_A}{k_BT}\right)\exp\left(-\frac{eE_Cd}{k_BT}\right)\right]p = G_{th}+G_{ph}, \tag{9}$$

where $j_{GL} = e\Sigma_{GL}/\tau_{esc}$ and $\mu_0 = (\Delta_C - \Delta_V)/2$. The term in the left-hand side of Eq. (9), proportional to the hole capture probability p, constitutes the rate of the capture of the holes injected from the contacts into the GL base. The first term, G_{th}, the right-hand side of this equation is the rate of the holes and electrons thermionic emission from the GL base:

$$G_{th} = \frac{j_{GL}}{e}\exp\left(-\frac{\Delta_G}{2k_BT}\right)\left[\exp\left(\frac{\mu_0-\mu}{k_BT}\right)-\exp\left(-\frac{\mu_0-\mu}{k_BT}\right)\exp\left(\frac{eE_Ed}{k_BT}\right)\right]. \tag{10}$$

The rate of thermionic emission from the GL-base, described by Eq. (10), comprises two terms associated with the holes and electrons, $G_{th,p}$ and $G_{th,n}$ (the first and the second terms, respectively). The exponential factor $\exp(eE_Ed/k_BT)$ appears due to the extra barrier in the EBL for the electrons being emitted from the GL-base at $E_E<0$ (see Fig. 1(a). The term G_{ph} in the right-hand side of Eq. (9) given by Eq. (5) is the rate of the hole photoescape from the GL-base.

The net current density corresponding to the hole and electron processes in question is given by

$$j = j_{GL}\exp\left(-\frac{\Delta_G}{2k_BT}\right)\times\left\{\exp\left(\frac{\mu_0+\mu_A}{k_BT}\right)\exp\left(\frac{eE_Ed}{k_BT}\right)-\exp\left(\frac{\mu_0+\mu_A}{k_BT}\right)\exp\left(-\frac{eE_Cd}{k_BT}\right)(1-p)-\frac{1}{2}\exp\left(\frac{\mu_0-\mu}{k_BT}\right)+\exp\left(-\frac{\mu_0-\mu}{k_BT}\right)\left[\exp\left(\frac{eE_Ed}{k_BT}\right)-\frac{1}{2}\exp\left(-\frac{eE_Cd}{k_BT}\right)\right]\right\}-\frac{e}{2}G_{ph}, \tag{11}$$

Different terms in the expression for the net current density given by Eq. (11) correspond to the fluxes at $x = 0$ of the holes and electrons thermoexcited from the GL base and to the flux of the photoexcited holes (the term $-eG_{ph}/2$). The factor 1/2 appears in the last quantity is because only one-half of the photoexcited holes goes to the emitter (and crosses the plane $x = 0$), while the other half of the photoexcited holes propagates toward the collector. In deriving of Eqs. (9) and (11), we have disregarded small contributions of the electrons injected from both the emitter and collector GLs $\Theta_{E,n}$ and $\Theta_{C,n}$ given by Eqs. (2). Indeed, according to Eqs. (1) and (2), $\Theta_{E,n}/\Theta_{E,p} = \Theta_{C,n}/\Theta_{C,p} = \exp[-2(\mu_0 + 2\mu_A)/k_BT] \ll 1$.

Optics EXPRESS

Combining Eqs. (9)–(11), we express the net current density as a function of the Fermi energy μ, the electric field E_E, and the radiation intensity I_Ω as follows:

$$\begin{aligned} j = j_{GL}\exp\left(-\frac{\Delta_G}{2k_BT}\right) \\ \times\left\{\left[\exp\left(\frac{\mu_0-\mu}{k_BT}\right)-\exp\left(-\frac{\mu_0-\mu}{k_BT}\right)\exp\left(\frac{eE_Ed}{k_BT}\right)\right]\left(\frac{1}{p}-\frac{1}{2}\right)\left[\frac{1-\exp(-eV/k_BT)}{1+\exp(-eV/k_BT)}\right]\right. \\ \left.+\frac{1}{2}\exp\left(-\frac{\mu_0-\mu}{k_BT}\right)\exp\left(\frac{eE_Ed}{k_BT}\right)[1-\exp(-eV/k_BT)]\right\} \\ +e\beta F_\Omega\xi_\Omega I_\Omega\left[\frac{1-\exp(-eV/k_BT)}{1+\exp(-eV/k_BT)}\right]\left(\frac{1}{p}-\frac{1}{2}\right). \end{aligned} \tag{12}$$

Simultaneously, for the case of weak irradiation (small I_Ω and, hence, small G_Ω) we obtain the following formula relating the electric field in the EBL E_E and the "dark" Fermi energy μ_{dark}:

$$\exp\left(\frac{eE_Ed}{k_BT}\right)=\frac{\exp[2(\mu_0-\mu_{dark})/k_BT]}{1+\exp[(2\mu_0+\mu_A-\mu_{dark}/k_BT]p[1+\exp(-eV/k_BT)]}. \tag{13}$$

4. Dark current gain and dark current-voltage characteristics

Using Eqs. (12) and (13), considering that the net current density comprises the dark current and photocurrent components $j = j_{dark} + j_{ph}$, and singling out the former one, we arrive at

$$j_{dark}=g_{dark}j_{GL}\exp\left(-\frac{\Delta_V+\mu_{dark}}{k_BT}\right)\left[\frac{1-\exp\left(-\frac{eV}{k_BT}\right)}{1+\exp\left(-\frac{eV}{k_BT}\right)}\right] \tag{14}$$

Here the quantity

$$g_{dark}=\left\{\frac{\exp\left(\frac{2\mu_0+\mu_A-\mu_{dark}}{k_BT}\right)p\left(\frac{1}{p}-\frac{1}{2}\right)+\frac{1}{2}}{1+\exp\left(\frac{2\mu_0+\mu_A-\mu_{dark}}{k_BT}\right)p\left[1+\exp\left(-\frac{eV}{k_BT}\right)\right]}\right\}\left[1+\exp\left(-\frac{eV}{k_BT}\right)\right] \tag{15}$$

constitutes the dark-current gain.

Taking into account a relative smallness of the electric field, E_E, in the EBL, in the most interesting situations $\mu \gg k_BT$ when $\mathcal{F}_1(\mu/k_BT) \simeq (\mu/k_BT)^2/2$, in the case of relatively small electric field in the EBL, Eq. (8) yields

$$\frac{\mu_{dark}}{k_BT}\simeq\frac{\mu_D}{k_BT}\left(1-\frac{V}{2V_D}\right)=\frac{\mu_D-\gamma eV}{k_BT}, \tag{16}$$

where $\gamma = \kappa\hbar^2v_W^2/8e^2d\mu_D$. Setting $\Sigma_A = \Sigma_D = 3.5\times10^{11}$ cm^2, using Eq (26) in Appendix A,which relates the density and the Fermi energy, one obtains $\mu_A \sim \mu_D \simeq 50$ meV and $\gamma = \kappa\hbar^2v_W^2/8e^2d\mu_D$. In such a case, assuming that, $\kappa = 4$ and $d \geq 10^{-5}$ cm, we find $V_A \sim V_D \simeq 1600$ mV and $\gamma \simeq 6.79\times10^{-3}$. It should be noted that $e|E_E|d<\max e|E_E|d = \mu_A+\mu_D$. Such a maximum is achieved in equilibrium ($V = 0$ and $G_\Omega = 0$). Hence, the quantity $\mu_D|E_Ed|/k_BTV_D<\mu_D(\mu_A+\mu_D)/k_BTV_D \sim 2\gamma(\mu_D/k_BT)$, so that the term with eE_Ed omitted in the right-side of Eq. (16) yields the correction of μ of the same order of magnitude as the quantum capacitance correction.

Optics EXPRESS

In line with Eq. (16), the dark current gain relates the dark current density j_{dark} and the rate of the thermionic hole emission from the GL $G_{ph,p} = \frac{j_{GL}}{e}\exp\left(-\frac{\Delta_V + \mu_D - \gamma\, eV}{k_BT}\right)$ (see Eq. (10)) with the hole activation energy $\varepsilon_{act} = \Delta_V + \mu_D - \gamma\, eV$. Consequently, considering that at practical bias voltages $\gamma\, eV < k_BT$, we obtain the current-voltage characteristic:

$$j_{dark} = g_{dark} j_{GL}\exp\left(-\frac{\Delta_V + \mu_D - \gamma\, eV}{k_BT}\right)\left[\frac{1 - \exp\left(-\frac{eV}{k_BT}\right)}{1 + \exp\left(-\frac{eV}{k_BT}\right)}\right]. \tag{17}$$

with

$$g_{dark} \simeq \frac{\exp\left(\frac{2\mu_0 + \mu_A - \mu_D}{k_BT}\right)p\left(\frac{1}{p} - \frac{1}{2}\right)\left[1 + \exp\left(-\frac{eV}{k_BT}\right)\right]}{1 + \exp\left(\frac{2\mu_0 + \mu_A - \mu_D}{k_BT}\right)p\left[1 + \exp\left(-\frac{eV}{k_BT}\right)\right]}. \tag{18}$$

The expressions for the dark Fermi energy $\mu_{dark}|_{V=V_0}$ and the current density $j_{dark}|_{V=V_0}$, following from the above formulas at the bias voltages close to the threshold voltage V_0 (when $E_E \simeq 0$) and the expression for quantity V_0 as a function of the GLIP structural parameters are derived in Appendix B. As demonstrated there, the threshold voltage V_0 and the threshold current density are rather large: $V_0 \sim V_D$ and $j_{dark}|_{V=V_0} \sim j_{GL}\exp[(\mu_A - \Delta_V)/k_BT]$. The latter value coincides with the maximum hole current density, which can be provided by the emitter under consideration with the given parameters Δ_V and μ_A.

As follows from Eq. (18), at moderate values of μ_0 (i.e., Δ_C close to Δ_V) and small capture probabilities, g_{dark} can be much smaller than $g = \left(\frac{1}{p} - \frac{1}{2}\right) \simeq \frac{1}{p}$. The effect of a relatively strong decrease in g_{dark} can called as the effect of the dark-current gain suppression (reduction). This effect is associated with the contribution of the electron thermionic emission from the GL-base to the carrier and charge balance in the GL-base, so that both the holes and electrons contribute to the GBIP operation. Contrary to the GBIPs with $\Delta_C \gtrsim \Delta_V$ (in the GBIPs with the b-P and b-As BLs under consideration $\Delta_C \simeq 2\Delta_V$), in similar IPs with $\Delta_C \gg \Delta_V$, i.e., with a large μ_0, exhibiting the monopolar operation, g_{dark} given by Eq. (18) turns to $g_{dark} \simeq 1/p$.

Figures 2 shows the dependence of the dark current gain g_{dark} on the capture probability p calculated for the GBIPs with the b-P and b-As BLs,with the different values of the GL-base Fermi energy μ_D at $T = 300$ K and $T = 200$ K calculated using Eq. (17). It is assumed that the emitter GL Fermi energy $\mu_A = 50$ meV and $V = 50$ mV. The dotted lines correspond to the dark-current gain in the GBIPs with the monopolar operation when the electron processes are insignificant. In this case, the pertinent gain $g_{dark} = g$. As shown in the following, g coincides also with the photoconductive gain g_{ph}. Such a dark-current gain is inherent to more customary GL, QW, and QD IPs [2].

Figure 2 confirms that in the GBIPs $g_{dark} < g$, particularly at small p when even $g_{dark} \ll g$. Comparing Figs. 2(a) and 2(b), one can see that the effect of the dark-current gain reduction is more pronounced in the GBIPs with the b-As BLs. This is because in such GBIPs, the energy barrier, Δ_C, for the electrons in the GL-base is smaller than in the GBIPs with the b-P BLs. Hence, the electron thermionic emission in the former GBIPs can be relatively strong provided that the electron activation energy $(\Delta_C - \mu_D)$ is sufficiently small.

Figure 3 shows the normalized current-voltage characteristics described by Eqs. (17) and (18) for different values of the Fermi energy μ_D at $T = 300$ K and $T = 200$ K. The emitter GL Fermi energy μ_A is assumed to be the same as in Fig. 2. The capture probability is set $p = 0.01$. The latter value is in line with the calculation results [40] related to the capture into GLs of the thermal carriers propagating in the BLs made of a similar material (WS_2).

Optics EXPRESS

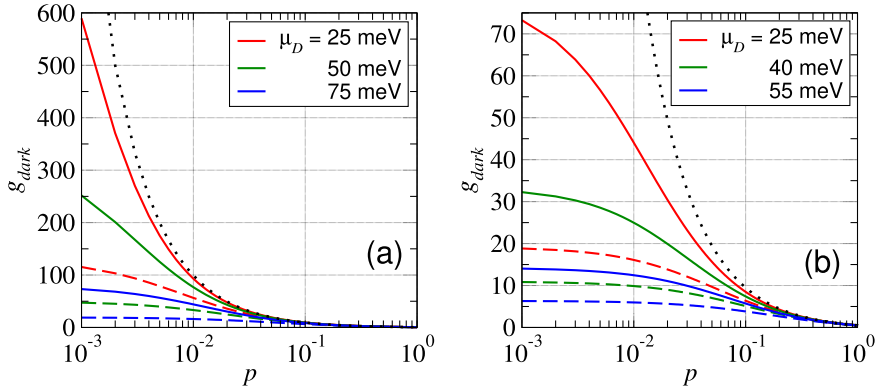

Fig. 2. The dark current gain g_{dark} versus the capture probability p for the GBIPs with different BLs: (a) with the b-P BL and (b) with the b-As BL. Dashed lines correspond to T = 300 K and solid lines correspond to T = 200K. Dotted lines correspond to $g = (1/p - 1/2)$.

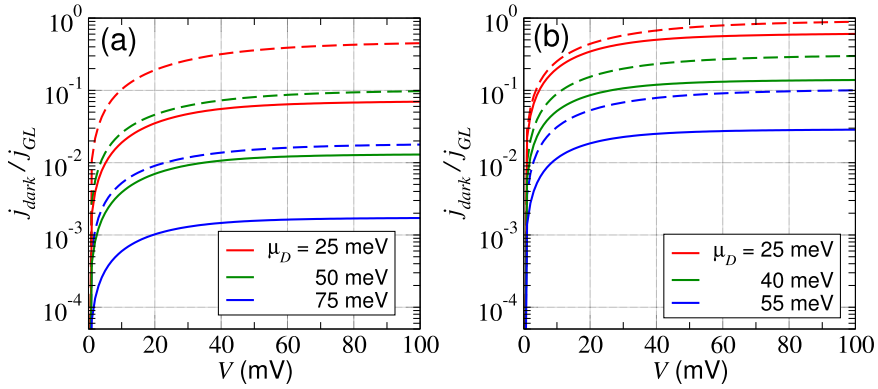

Fig. 3. The normalized dark current j_{dark}/j_{GL} versus bias voltage V for the GBIPs with (a) b-P BLs and (b) b-As BLs at T = 300K (dashed lines) and T = 200 K (solid lines) calculated for different Fermi energies μ_D.

On can see from Fig. 3 that a decrease in the temperature leads to a substantial lowering of the dark current. This is attributed to a lesser rate of the hole thermionic emission from the GL-base at lower temperatures. However a lowering of the dark current with decreasing temperature is somewhat weaker than that described by the exponential factor $\exp[-(\Delta_V + \mu_D/k_BT]$ with $(\Delta_V + \mu_D)$ being the hole activation energy. This is because lower temperatures correspond to a larger dark-current gain g_{dark}. Thus, a decrease in $\exp[-(\Delta_V + \mu_D/k_BT]$ is partially compensated by an increase in g_{dark}. As for the dark current in the GDIPs with the b-As BLs corresponding to smaller activation energies $(\Delta_C - \mu_D)$ and $(\Delta_V + \mu_D)$ for the electrons and holes in the GL-base, Fig. 3(b) shows a much smaller temperature variation of the dark current. This is due to a more marked role of the dark-current gain reduction.

Optics EXPRESS

5. GBIP detector responsivity

At a weak irradiation, Eq. (12) yields the following expression for the photocurrent density:

$$j_{ph} = g_{ph} e\beta F_\Omega \xi_\Omega I_\Omega \left[\frac{1-\exp\left(-\frac{eV}{k_BT}\right)}{1+\exp\left(-\frac{eV}{k_BT}\right)}\right]. \tag{19}$$

Here

$$g_{ph} = \left(\frac{1}{p} - \frac{1}{2}\right) \simeq \frac{1}{p} \tag{20}$$

is photoconductive gain, which is the ratio of the net photocurrent density j_{ph} and the rate of the hole photoescape from the GL $\beta F_\Omega \xi_\Omega I_\Omega$ multiplied by the carrier charge e. According to Eqs. (6) and (8), for the factor F_Ω one can use its value in the dark conditions given by the following formula:

$$F_\Omega = \frac{1}{\exp[(\mu_{dark} - \hbar\Omega/2)/k_BT] + 1} \simeq \frac{1}{\exp[(\mu_D - \gamma V - \hbar\Omega/2)/k_BT] + 1}.$$

In the situations corresponding to the formulas derived in the previous sections $|E_E| \ll E_C \simeq V/d$, ξ_Ω described by Eq. (7) can be presented as

$\xi_\Omega = (1 + \tau_{esc}/\tau_{relax})^{-1}$ at $\hbar\Omega \geq 2\Delta_V$, and $\xi_\Omega = \left\{1 + \frac{\tau_{esc}}{\tau_{relax}} \exp\left[\frac{dE_T}{V}\left(1 - \frac{\hbar\Omega}{2\Delta_V}\right)^{3/2}\right]\right\}^{-1}$ at $\hbar\Omega \leq 2\Delta_V$, where $E_T = (4\sqrt{2m_z}\Delta_V^{3/2}/3e\hbar)$.

The internal detector responsivity, determined as $R_\Omega = j_{ph}/\hbar\Omega I_\Omega$, is given by

$$R_\Omega \simeq g_{ph} \frac{e\beta F_\Omega \xi_\Omega}{\hbar\Omega} \left[\frac{1-\exp\left(-\frac{eV}{k_BT}\right)}{1+\exp\left(-\frac{eV}{k_BT}\right)}\right], \tag{21}$$

At moderate bias voltages when the hole tunneling from the GL-base is insignificant, Eq. (20) gives the following spectral dependence of the GBIP responsivity:

$$R_\Omega \simeq R \frac{g_{ph}}{(1 + \tau_{esc}/\tau_{relax})} \frac{g_{ph}\left(\frac{2\Delta_V}{\hbar\Omega}\right)}{\left[\exp\left(\frac{\mu_D - \hbar\Omega/2}{k_BT}\right) + 1\right]} \tag{22}$$

with the maximum at $\hbar\Omega_{max} \sim 2\mu_D$. Here $R = (e\beta/2\Delta_V)$. For the GBIPs with the b-P BLs, $\beta = 0.023/2$, $p = 0.005 - 0.01$, $\tau_{esc}/\tau_{relax} = 0.1$, and $\mu_D = 50$ meV, at $T = 300$ K, $\hbar\Omega = 200$ meV, and $V = 100$ mV, Eq. (21) yields $R_\Omega \simeq 3.68 - 7.36$ A/W. In the GLIPs with the b-As BLs at $\hbar\Omega = 100$ meV and the same voltage, one obtains $R_\Omega \simeq 5.04 - 10.08$ A/W.

At elevated bias voltages, the photoexcited holes tunneling leads to the reinforcement of the net rate of the hole photoescape. This can markedly affect the GBIP spectral characteristics in the range $\hbar\Omega < 2\Delta_V$. Figure 4, based on Eq. (21), shows the responsivities of the GBIPs with the b-P and b-As BLs as function of the photon energy $\hbar\Omega$ and the carrier Fermi energy in the GL-base μ_D. The latter is related to the donor density in the GL-base approximately as $\mu_D \propto \sqrt{\Sigma_D}$. It is assumed that $\beta = 0.023/2$, $\tau_{esc}/\tau_{relax} = 0.1$, $p = 0.01$, $T = 300$ K, and $V = 1$ V. In determining of the tunneling voltage dE_T we put $d = 10^{-5}$ cm, $m_z \gtrsim 2.5 \times 10^{-28}$ g (in line

Optics EXPRESS

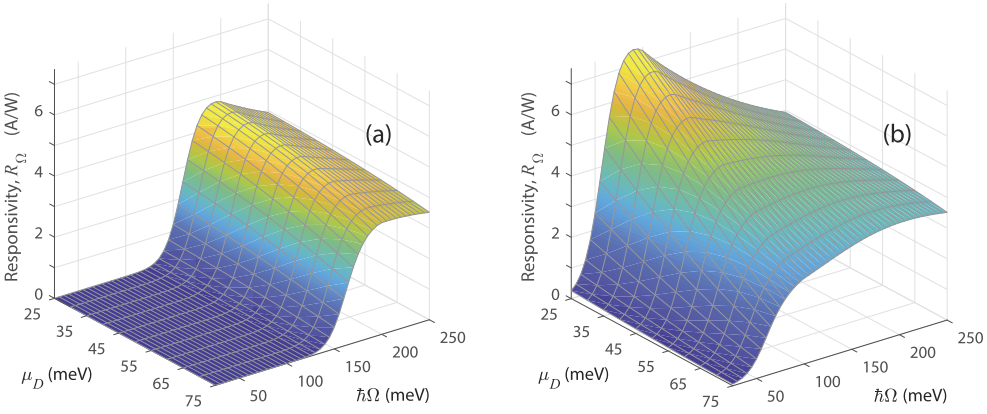

Fig. 4. The GBIP responsivity R_Ω versus the photon energy $\hbar\Omega$ and Fermi energy μ_D (donor density in the GL-base) for (a) b-P BLs (μ_A = 100 meV, dE_T = 3 V, and V = 1 V) and (b) b-As (μ_A = 50 meV, dE_T = 1 V, and V = 1 V).

with the experimental data [13,14]; see also the review [46]). As a result, for the GBIPs with the b-P and b-As BLs we have dE_T = 3 V and dE_T = 1 V, respectively.

As seen from Fig. 4, the GBIP responsivity exhibits a maximum at the photon energy $\hbar\Omega \simeq 2\Delta_V$, i.e., at $\hbar\Omega = \hbar\Omega_{max} \simeq 200$ meV ($\lambda \simeq 6$ μm) in the case of the b-P BLs and at $\hbar\Omega \simeq 100$ meV ($\lambda \simeq 12$ μm) in the case of the b-As BLs. At small smaller photon energies $\hbar\Omega < \hbar\Omega_{max}$, the responsivity drops but can be substantial. The GBIP response at $\hbar\Omega < \hbar\Omega_{max}$ is associated with the tunneling of the photoexcited holes. Since the tunneling probability increases with increasing $E_C \simeq V/d$, the width of the spectral range where the responsivity remains relatively large increases with increasing bias voltage V. This is seen from Fig. 5, which demonstrates how the responsivity spectral characteristics of the GBIP with the b-As BLs change with varying bias voltage V at different temperatures (μ_A = 50 meV, μ_D = 50 meV, and dET = 1000 mV). As follows from Fig. 5, the responsivity can reach the values $R_\Omega \sim 10.5$ A/W in the case of fairly low photon energies $\hbar\Omega \lesssim 25$ meV ($\lambda \gtrsim 48$ μm or $\Omega/2\pi \lesssim 6$ THz. The latter might be possible at sufficiently large bias voltages but smaller that the threshold voltage V_0 (see Fig. 6). An increase in the responsivity at the photon energies $\hbar\Omega \gtrsim \hbar\Omega_{max}$ increasing voltages is associated with a

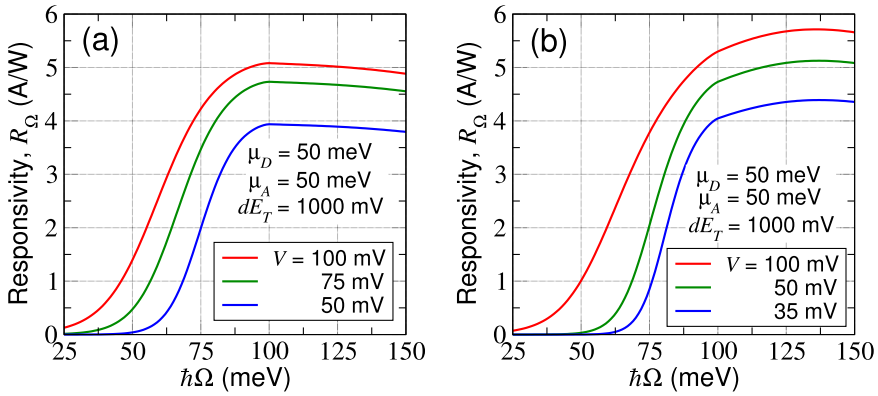

Fig. 5. Variation of the GBIP (with the b-As BLs) spectral characteristics with varying bias voltages V at (a) T = 300 K and (b) T = 200 K.

Optics EXPRESS

weakening of the hole injection from the collector GL corresponding to the right-side factor in Eq. (21).

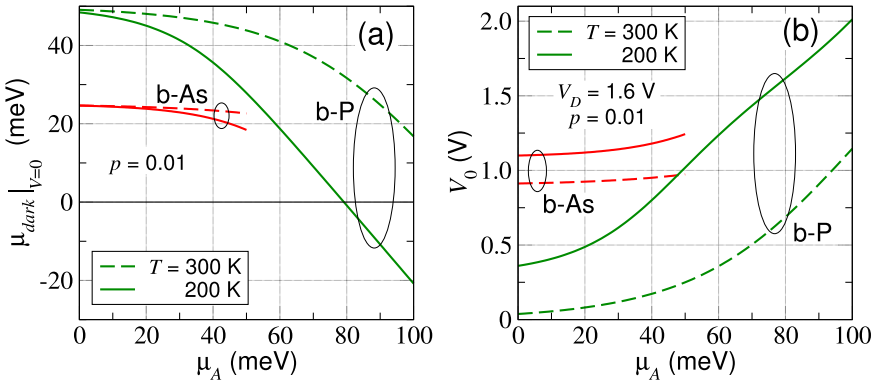

Fig. 6. (a) The Fermi energy in the GL-base $\mu_{dark}|_{V=V_0}$ at the threshold voltage V_0 and (b) the threshold voltage V_0 as function of the Fermi in the emitter GL μ_A at fixed V_D (fixed $\mu_D = 50$ meV).

6. GBIP dark-current limited detectivity

We estimate the GBIP dark-current-limited detectivity D^*_Ω using the following general formula (see, for example, [47–49]):

$$D^*_\Omega = \frac{G_{ph}}{2\hbar\Omega\, I_\Omega \sqrt{G_{th}}}. \tag{23}$$

Considering Eqs. (5), (10), and (13), from Eq. (23) we arrive at the following formula for the GDIP dark-current limited (or thermally-limited) GBIP detectivity:

$$D^*_\Omega = \frac{\beta\, F_\Omega \xi_\Omega}{2\hbar\Omega}\sqrt{\frac{e}{j_{GL}}}\exp\left(\frac{\Delta_V + \mu_D}{2k_BT}\right)\sqrt{1+K}. \tag{24}$$

Here $K = \dfrac{1}{p}\exp\left(\dfrac{\Delta_V - \Delta_C - \mu_A + \mu_D}{k_BT}\right)$ characterizes the effect of the dark-current gain reduction on the detectivity.

As follows from Eq. (24), in the case $K \ll 1$, which corresponds to large values of Δ_C when the operation of the GLIP under consideration is associated solely with the hole processes,

$$D^*_\Omega \simeq \overline{D^*_\Omega} = \frac{\beta\, F_\Omega \xi_\Omega}{2\hbar\Omega}\sqrt{\frac{e}{j_{GL}}}\exp\left(\frac{\Delta_V + \mu_D}{2k_BT}\right). \tag{25}$$

For the GBIPs with the b-As BLs, $j_{GL}/e = 10^{21} - 10^{22}$ cm^{-2}s^{-1}, and $\mu_D = 50$ mev for $\hbar\Omega = 2\Delta_V = 100$ meV, we obtain for the characteristic detectivity $\overline{D^*_\Omega} \simeq (2.5 - 7.9)\times 10^7$ cm$\sqrt{\text{Hz}}$/W and $\overline{D^*_\Omega} \simeq (6.6 - 20.8)\times 10^7$ cm$\sqrt{\text{Hz}}$/W at $T = 300$ K and $T = 200$ K, respectively.

In the GBIP under consideration with the decreased dark current, particularly those with the b-As BLs, the value K can be large. In this case, the GBIP detectivity $D^*_\Omega = \overline{D^*_\Omega}\sqrt{1+K}$ can markedly exceed $\overline{D^*_\Omega}$. Indeed, setting $\Delta_C = 100$ meV, $\Delta_V = \mu_A = \mu_D = 50$ meV and $p = 0.01$, for $T = 300$ K, we obtain $\sqrt{1+K} \simeq 3.9$. At smaller p and μ_A, the quantity $\sqrt{1+K}$ can even larger. In particular, for $\mu_A = 25$ meV and $p = 0.005$, $\sqrt{1+K} \simeq 8.8$ at $T = 300$ K and $\sqrt{1+K} \simeq 6.9$ at $T = 200$ K. Accordingly, we find and $D^*_\Omega \simeq (1 - 7)\times 10^8$ cm$\sqrt{\text{Hz}}$/W and $D^*_\Omega \simeq (3 - 14)\times 10^8$ cm$\sqrt{\text{Hz}}$/W.

Optics EXPRESS

The characteristic detectivity $\overline{D^*_\Omega}$ substantially increases with decreasing temperature. However, a decrease in the temperature leads to a decrease in the parameter K, so that at lowered temperatures one obtains $D^*_\Omega \gtrsim \overline{D^*_\Omega}$.

Equation (26) indicates that the dark-current limited responsivity D^*_Ω decreases with increasing μ_A and increasing μ_D. However, an increase in μ_D beyond Δ_V, leads to a decrease in the GL absorption coefficient at $\hbar\Omega = 2\Delta_V$ associated with the Pauli blocking of the interband transitions (decrease in the factor F_Ω). All this implies that the variation of the GL doping can be used for the GBIP optimization.

7. Discussion

(i) In the range of elevated bias voltages $V \gtrsim V_0$ (E_E>0), the hole current injected from the emitter becomes close to its maximum value provided by this emitter. It implies that at such bias voltages the current-voltage characteristics saturate. The reinstatement of the injected hole current rise with increasing voltage is possible at fairly high voltages, at which μ_E exhibits a marked increase according to Eqs. (1) and (3). In the case of μ_A is close to Δ_V, i.e., the valence band of the EGL is filled by holes , or in the case of the bulk emitter, the injection current might be limited by the space charge of the holes propagating across the EBL. However, this can be important when $V \gtrsim V_0$.

(ii) The obtained formulas for the dark current are valid if j_{dark}<j_{GL}. Considering Eqs. (17) and (18), this inequality is equivalent to $(\Delta_C - 2\Delta_V)$<$2\mu_D - \mu_A$. Since $\Delta_C = 2\Delta_V$, the above inequalities are realized at $2\mu_D$>μ_A. For realistic values of μ_A<max$\mu_A = \Delta_V$, one obtains μ_D>50 meV and μ_D>25 meV for the b-P and b-As BLs. These conditions were satisfied in the above calculations. At μ_A substantially smaller than Δ_V, the inequalities in question are valid in very wide range of the GL-base doping levels. At fairly high photon energies ($\hbar\Omega$>Δ_G = 300 meV for b-P BLs and $\hbar\Omega$>Δ_G = 150 meV for b-As BLs), the photogeneration of both holes and electrons associated with the interband transitions in the BLs can provide an extra increase in the responsivity affecting the spectral characteristics at such photon energies. The pertinent generalization of Eq. (21) is rather trivial, but we believe that it is redundant.

(iii) It might be shown that the characteristics of the GBIPs with the bulk p^+ contact are similar to those obtained above. In particular, to adjust the above formulas for the case of the GBIPs with bulk contacts made of the p^+-doped regions of the same materials as the BLs , one need just to set $\mu_E = \mu_C = \mu_A = \Delta_V$ in Eq. (1) and the following equations.

(iv) In our model we disregarded the contribution of the thermalized electron and hole tunneling to the emission from the GL-base assuming that the latter is weaker in comparison with the thermionic emission. In the voltage range V<V_0 mainly considered above, the electric field in the EBL is small, whereas it can be relatively large in the CBL. In such a case, the net rate of the hole escape from the GL-base can comprise a tunneling component. As a result, the voltage point, at which the hole and electron escapes from the GL-base are balanced, somewhat shifts.

However, the rate of thermalized carrier tunneling escape is small in comparison with the rate of their thermionic escape from the GL if the following inequalities are hold:

$$\exp\left(-\frac{\Delta_G}{2k_BT}\right) \gg \exp\left[-\frac{4d\sqrt{2m_z}}{3e\hbar}\left(\frac{\Delta_G}{2}\right)^{3/2}\right] = \exp\left[-\frac{2dE_T}{3e\hbar V}\left(\frac{\Delta_G}{\Delta_V}\right)^{3/2}\right]$$

or

$$\frac{eV}{k_BT} < \frac{4d\sqrt{m_z\Delta_G}}{3\hbar}.$$

For the b-As and b-P BLs of thickness $d = 10^{-5}$ cm, setting, $m_z \gtrsim 2.5 \times 10^{-28}$ g [13,14,45], the above inequality is satisfied when (eV/k_BT)<80 and (eV/k_BT)<150, respectively. At T = 200 and 300 K, one obtains V<1.3 − 2.5 V and V<2.5 − 3.75 V, and these inequalities were satisfied.

Optics EXPRESS

(v) It appears reasonable to compare the GBIP performance with the performance of the QWIPs and QDIPs for the same spectral range $\lambda \sim 8 - 12\mu$m. Such QWIPs and QDIPs are considered as effective as building blocks for FIR cameras, GHz-frequency heterodyne receivers, and other devices [1–3,50–54]. In contrast to the GBIPs, the QWIPs and QDIPs use the intersubband (intraband) carrier transitions from the QWs and QDs. Due to a stronger interband radiation absorption in the GBIPs in comparison with the intraband absorption in the QWIPs and QDIPs, the internal GBIP responsivity R_Ω can be much higher (about one order of magnitude) than the internal QWIP responsivity R_Ω^{QWIP}. A smaller carrier capture probability into the GLs p (in the GBIPs under consideration) [40] than the carrier capture probability into the QWs p^{QW} (in QWIPs) provides an additional increase in the ratio R_Ω/R_Ω^{QWIP}. A detailed comparison of the responsivity of the GBIP (with a large difference between Δ_C and Δ_V in which the effect of the partial dark current gain suppression does not reveals) and the QWIPs was conducted by us previously [25]. The results of [25] are also valid for the GBIPs studied above. Due to the GBIP sensitivity to the normally incident radiation associated with the using the interband transitions, there is no needs to use extra coupling system like gratings. This also contributes to the advantages of the GBIPs over the QWIPs, in which such coupling system (at least in n-type QWIPs) is indispensable. The utilization of various resonant couplers (see, for example, [55,56]), can provide a substantial increase in the responsivities of the QWIPs and GBIPs to the same extent. A weaker carrier capture and, hence, a larger photoconductive gain in QD arrays in comparison to QWs can enable a higher QDIP responsivity R_Ω^{QDIP} [48,49,57]. A relatively strong interband absorption in the GBIPs can provide markedly large ratios R_Ω/R_Ω^{QDIP} (compare the estimates of R_Ω in Sec. 5 and the data from Fig. 5 with the results of [60,61], where R_Ω^{QDIP} about a few A/W was achieved (see also [3]).

(vi) As predicted, a stronger radiation interband absorption in the GLs in comparison with the intraband intersubband absorption in the QWs and the QD arrays as well as the the possibility of the dark current suppression in the GBIPs revealed above, implies that the GBIPs with b-B and b-As BLs under consideration can surpass the QWIPs and QDIPs in the dark-current limited detectivity. This is true at least for the single-QW QWIPs and the single-QD array QDIPs, particularly, at elevated temperatures (higher than nitrogen temperatures).

Using the value of the GBIP detectivity at $T = 300$ K estimated in Sec. 6 $D_\Omega^* \simeq (1 - 7) \times 10^8$ cm$\sqrt{\text{Hz}}$/W and comparing with the recent experimental value for a QWIP consisting of five QWs [54] $D_\Omega^{*QWIP} \simeq 2.8 \times 10^7$ cm$\sqrt{\text{Hz}}$/W, we find $D_\Omega^*/D_\Omega^{*QWIP} \simeq 3.6 - 25.0$. Thus, the GBIP under consideration (with a single-GL base) markedly surpass the QWIP (with five QWs) used in [54]. One needs to stress that $D_\Omega^{*QWIP} \propto \sqrt{N} \gg 1$ (for example, [2]). Considering this one can find that the ratio of the detectivities per one active layer is even larger: $\sqrt{N}D_\Omega^*/D_\Omega^{*QWIP} \simeq 8 - 56$.

Comparing the GBIP and QDIP detectivities, we use the estimate obtained in Sec. 6 for the GBIPs ($D_\Omega^* \simeq 1.4 \times 10^9$ cm$\sqrt{\text{Hz}}$/W) and the date for QDIPs at $T = 200$ extracted from 58,59: $D_\Omega^{*QDIP} \simeq 6 \times 10^9$ cm$\sqrt{\text{Hz}}$/W for the QDIP with the number of the QD arrays $N = 70$ [58] and $D_\Omega^{*QDIP} \simeq 1 \times 10^9$ cm $\sqrt{\text{Hz}}$/W for the QDIP with $N = 20$ [59] QD arrays (respectively $D_\Omega^{*QDIP} \simeq 6 \times 10^9$ cm $\sqrt{\text{Hz}}$/W. We also account for that $D_\Omega^{*QDIP} \propto \sqrt{N}$ [58]. As a result, we find that $\sqrt{N}D_\Omega^*/D_\Omega^{*QWIP} \simeq 2 - 6$. Thus, the GBIPs markedly surpass the QWIP and the QDIPs in responsivity, while the GBIPs being based on a number of the floating GLs forming the GBIP base might prevail the QWIP and the QDIPs also in the detectivity. A variety of the structural parameters determining the GBIP characteristics allows wide opportunities for the GBIP optimization, which can result in a marked enhancement of the detectivity.

The comparatively high GBIP detectivity is attributed to the following three factors: a stronger absorption due to the interband transitions, a larger activation energy of the carrier thermionic emission from the GL (equal to $\Delta_V + \mu_D$) , and a dark current gain reduction (leading to the appearance of the factor $\sqrt{1 + K}$. According to Eq. (25), the rate of the carrier thermionic emission

Optics EXPRESS

is characterized by an exponential factor $\exp[(\Delta_V + \mu_D)/2k_BT] \simeq \exp[(\hbar\Omega/2 + \mu_D)/2k_BT]$. The thermionic emission from the QWs in the QWIPs and from the QD array in the QDIPs can be characterized by the activation energy $\hbar\Omega + \mu_D$ and $\hbar\Omega$, respectively. Hence, the pertinent factors in the QWIP and the QDIP detectivities are $\exp[(\hbar\Omega - \mu_D)/2k_BT]$ (see, for example, [2]) and $\exp[(\hbar\Omega)/2k_BT]$ (see, for example, [2] and [57–59]). Considering this, we find

$$\frac{D^*_\Omega}{D^{*QWIP}_\Omega} \propto \frac{r\sqrt{1+K}}{\sqrt{N}} \exp\left(\frac{4\mu_D - \hbar\Omega}{4k_BT}\right), \qquad \frac{D^*_\Omega}{D^{*QDIP}_\Omega} \propto \frac{r\sqrt{1+K}}{\sqrt{N}} \exp\left(\frac{2\mu_D - \hbar\Omega}{4k_BT}\right),$$

where $r \gg 1$ is the ratio of the absorption coefficients in the GL and the QW (or the QD array). If $\mu_D = 50$ meV and $\hbar\Omega = 100$ meV (as in the estimates of D^*_Ω used above) at $T = 200$ K and $T = 300$ K, the above exponential factor is approximately equal to 4.3 and 2.6, respectively. Since in reality $r/\sqrt{N}>1$ or even $r/\sqrt{N} \gg 1$, there should be $D^*_\Omega/D^{*QWIP}_\Omega \gg 1$.

(vii) The high-frequency properties of the GBIPs as well as the QWIPs [52–54,60] are important for some of their application, in particular for the GHz heterodyne detection. These properties of the GBIPs are determined by the same parameters as those of the QWIPs [61,62], namely, the time of the carrier (hole) transit across the BL $\tau_{tr} = d/v_d$ (v_d is the hole velocity over the BL) and the characteristic carrier capture time $\tau_c = \tau_{tr}/p \gg tau_{tr}$. At the signal frequencies $\omega \lesssim \tau_c^{-1} \ll \tau_{tr}^{-1}$, the GL recharging manages to vary the hole injection from the EGL, so at such signal frequencies the effect of the photoconducting gain works. In this case, the GBIP high-frequency responsivity $R^\omega_\Omega \simeq R_\Omega \propto g_{ph}$. In the signal frequency range $\tau_c^{-1}<\omega<\tau_{tr}^{-1}$, the recharging of the GL base does not follow the variation of the incident radiation, so that the photoconductive gain disappears. In this signal frequency range $R^\omega_\Omega<R_\Omega$. At relatively high signal frequencies $\omega>\tau_{tr}^{-1}$, the GBIP responsivity steeply drops. Thus, the highest operating frequency of the GBIPs is limited by τ_{tr}^{-1}. For the realistic thicknesses of the BLs used in the estimates above $d = 10^{-5}$, assuming that $v_d = (10^6 - 10^7)$ cm/s, we obtain $f_{max} \simeq v_d/2\pi\, d \simeq (16 - 160)$ GHz. Hence, the GBIPs (as the QWIPs) can be used for the GHz-frequency heterodyne receivers operating at elevated temperatures (including the room temperature).

8. Conclusions

We evaluate the characteristics of the GBIPs based the heterostructures with the b-P and b-As BLs and the GL-base. The GBIPs can operate in the range of the wavelengths longer than the photodetectors using the interband transitions in the b-P and b-As, i.e., in the wavelengths $\lambda \gtrsim (6 - 12)$ μm. The spectral range of the GBIP operation can be varied using the b-As_xP_{1-x} compounds. We demonstrated that the GBIP characteristics are very sensitive to the structural parameters, particularly, to the GL-base doping and to the bias voltage. An enhancement of the GL-base doping can lead to a significant reduction of the dark-current gain, preserving, nevertheless, the high values of the photoconductive gain. This enables the elevated GBIP responsivity combined with the moderate dark current and, therefore, the elevated dark-current limited detectivity. The optimized GBIPs performance might substantially surpass that of the QWIPs and QDIPs based on the standard materials and exploiting the intersubband transitions in the QWs and QDs, as well as other FIR and MIR photodetectors, particularly, at elevated temperatures.

Appendix A. Charge density versus Fermi energy in the GL-base

The electron and hole dispersion laws in GLs are given by the following linear relations [5]: $\varepsilon_n = +pv_W$ and $\varepsilon_p = -pv_W$, where p is the momentum and $v_W \simeq 10^8$ cm/s is the carrier characteristic velocity. Hence, the electron and hole systems in the GL in the dark are characterized

Optics EXPRESS

by the Fermi distribution functions in in the form:

$$f_n = \left[\exp[\left(\frac{pv_W - \mu}{k_BT}\right) + 1\right]^{-1}, \qquad f_p = \left[\exp\left(\frac{pv_W + \mu}{k_BT}\right) + 1\right]^{-1}.$$

Here (as in the main text) the Fermi energy is counted from the Dirac point.

The carrier charge density $e\Sigma$ in GLs is related to the Fermi energy μ as follows:

$$\begin{aligned} e\Sigma = \frac{2e}{\pi\hbar^2}\int_0^\infty dpp\left[\frac{1}{\exp\left(\frac{pv_W + \mu}{k_BT}\right) + 1} - \frac{1}{\exp\left(\frac{pv_W - \mu}{k_BT}\right) + 1}\right] \\ = \frac{2eT^2}{\pi\hbar^2 v_W^2}\left[\mathcal{F}_1\left(-\frac{\mu}{k_BT}\right) - \mathcal{F}_1\left(\frac{\mu}{k_BT}\right)\right], \end{aligned} \tag{26}$$

where

$$\mathcal{F}_1(a) = \int_0^\infty \frac{d\xi\xi}{\exp(\xi - a) + 1}$$

is the Fermi-Dirac integral [43,44]. At $\mu>0$ when the electron component in the GL dominates, $e\Sigma<0$. In the opposite case, the holes are the majority carriers in the GL.

If the absolute value of the Fermi energy $|\mu|$ is small, $\mathcal{F}_1(\mu/k_BT) - \mathcal{F}_1(-\mu/k_BT) \simeq 4\ln 2(\mu/k_BT)$. In the case $|\mu| \gg k_BT$, $\mathcal{F}_1(|\mu|/k_BT) \simeq (\mu/k_BT)^2/2$ and $\mathcal{F}_1(-|\mu|/k_BT) \ll 1$.

Appendix B. Calculation of the threshold Fermi energy, voltage, and dark current density

Setting $E_E = 0$ and $I_\Omega = 0$ and taking into account that in such a case $\mu_E = \mu_A$, one obtains the following equation governing $\mu_{dark}|_{V=V_0}$:

$$p\exp\left(\frac{\mu_A + \mu_0}{k_BT}\right) = 2\sinh\left(\frac{\mu_0 - \mu_{dark}|_{V=V_0}}{k_BT}\right), \tag{27}$$

so that

$$\mu_{dark}|_{V=V_0} = \mu_0 - k_BT\ln\left\{\frac{p}{2}\exp\left(\frac{\mu_A + \mu_0}{k_BT}\right) + \sqrt{\left[\frac{p}{2}\exp\left(\frac{\mu_A + \mu_0}{k_BT}\right)\right]^2 + 1}\right\}. \tag{28}$$

In addition, Eq. (8) at $V = V_0$, i.e., at $E_E = 0$, reads

$$V_0 = V_D + V_T\left[\mathcal{F}_1\left(-\frac{\mu_{dark}|_{V=V_0}}{k_BT}\right) - \mathcal{F}_1\left(\frac{\mu_{dark}|_{V=V_0}}{k_BT}\right)\right]. \tag{29}$$

As a result, from Eqs. (13), (29), and (30) we arrive at the following formula for the threshold dark current density:

$$\begin{aligned} j_{dark}|_{V=V_0} = \frac{e\Sigma_G}{\tau_{esc}}\exp\left(-\frac{\Delta_G}{2k_BT}\right)\left\{\left(1 - \frac{p}{2}\right)\exp\left(\frac{\mu_A + \mu_0}{k_BT}\right)\right. \\ \left. + \frac{1}{2}\left\{\frac{p}{2}\exp\left(\frac{\mu_A + \mu_0}{k_BT}\right) + \sqrt{\left[\frac{p}{2}\exp\left(\frac{\mu_A + \mu_0}{k_BT}\right)\right]^2 + 1}\right\}^{-1}\right. \\ \simeq \frac{e\Sigma_G}{\tau_{esc}}\exp\left(-\frac{\Delta_G}{2k_BT}\right)\left\{\left(1 - \frac{p}{2}\right)\exp\left(\frac{\mu_A + \mu_0}{k_BT}\right) = \frac{e\Sigma_G}{\tau_{esc}}\left(1 - \frac{p}{2}\right)\exp\left(\frac{\mu_A - \Delta_V}{k_BT}\right).\right. \end{aligned} \tag{30}$$

The right-hand side term in Eq. (30) only slightly smaller than the maximum hole current density from the emitter. This implies that at $V>V_0$, the hole current from the GL-based emitter under consideration is close to the saturation.

Optics EXPRESS

The Fermi energy $\mu_{dark}|_{V=V_0}$ and the characteristic voltage V_0 as functions of μ_A, i.e., the emitter and collector GLs doping level were calculated numerically using Eqs. (29) and (30). As an example, Fig. 6 shows the results of these calculations for GBIPs with b-As and b-B BLs at $T = 300$ K and $T = 200$ K. The following parameters were assumed: $p = 0.01$, $V_D = 1600$ mV (i.e., $\mu_D = 50$ meV) , $V_T = 494$ mV ($T = 300$ K) and $V_T = 220$ mV ($T = 200$ K), respectively. The quantity μ_A varies from $\mu_A = 0$ to $\mu_A = 100$ meV (for a GBIP with b-P BLs) and to $\mu_A = 50$ meV (for a GLIP with b-As BLs). The latter corresponds to the maximum acceptor densities $\Sigma_A = (3.5 - 7.0) \times 10^{11}$ cm^{-2}).

Funding

Japan Society for the Promotion of Science (16H06361); Research Institute of Electrical Communication, Tohoku University; Office of Naval Research.

Disclosures

The authors declare that there are no conflicts of interest related to this article.

References

1. A. Rogalski, "Infrared and Terahertz Detectors," (CRC Press, 2018).
2. H. Schneider and H. C. Liu, "Quantum Well Infrared Photodetectors: Physics and Applications," (Springer, 2007).
3. C. Downs and T. E. Vandervelde, "Progress in infrared photodetectors since 2000," Sensors **13**(4), 5054–5098 (2013).
4. M. Tonouchi, "Cutting-edge terahertz technology," Nat. Photonics **1**(2), 97–105 (2007).
5. A. H. Castro Neto, F. Guinea, N. M. R. Peres, K. S. Novoselov, and A. K. Geim, "The electronic properties of graphene," Rev. Mod. Phys. **81**(1), 109–162 (2009).
6. T. Mueller, F. N. A. Xia, and P. Avouris, "Graphene photodetectors for high speed optical communications," Nat. Photonics **4**(5), 297–301 (2010).
7. V. Ryzhii, M. Ryzhii, V. Mitin, and T. Otsuji, "Terahertz and infrared photodetection using p-i-n multiple-graphene layer structures," J. Appl. Phys. **107**(5), 054512 (2010).
8. F. Bonaccorso, Z. Sun, T. Hasan, and A. C. Ferrari, "Graphene photonics and optoelectronics," Nat. Photonics **4**(9), 611–622 (2010).
9. V. Ryzhii, N. Ryabova, M. Ryzhii, N. V. Baryshnikov, V. E. Karasik, V. Mitin, and T. Otsuji, "Terahertz and infrared photodetectors based on multiple graphene layer and nanoribbon structures," Opto-Electron. Rev. **20**(1), 15–25 (2012).
10. A. Tredicucci and M. S. Vitielo, "Device concepts for graphene-based terahertz photonics," IEEE J. Sel. Top. Quantum Electron. **20**(1), 130–138 (2014).
11. A. Rogalski, "Graphene-based materials in the infrared and terahertz detector families: a tutorial," Adv. Opt. Photonics **11**(2), 314–379 (2019).
12. R. W. Keyes, "The electrical properties of black phosphorus," Phys. Rev. **92**(3), 580–584 (1953).
13. A. Morita, "Semiconducting black phosphorus," Appl. Phys. A **39**(4), 227–242 (1986).
14. H. Asahina and A. Morita, "Band structure and optical properties of black phosphorus," J. Phys. C: Solid State Phys. **17**(11), 1839–1852 (1984).
15. Ling Xi, "The renaissance of black phosphorus," Proc. Natl. Acad. Sci. U. S. A. **112**(15), 4523–4530 (2015).
16. F. Xia, H. Wang, and Y. Jia, "Rediscovering black phosphorous as an anisotropic layered material for optoelectronics and electronics," Nat. Commun. **5**(1), 4458 (2014).
17. Z. Guo, H. Zhang, S. Lu, Z. Wang, S. Tang, J. Shao, Z. Sun, H. Xie, H. Wang, X.-F. Yu, and P. K. Chu, "From black phosphorus to phosphorene: Basic solvent exfoliation, evolution of Raman scattering, and applications to ultrafast photonics," Adv. Funct. Mater. **25**(45), 6996–7002 (2015).
18. B. Liu, M. Kopf, A. N. Abbas, X. Wang, Q. Guo, Y. Jia, F. Xia, R. Weihrich, F. Bachhuber, F. Pielnhofer, H. Wang, R. Dhall, S. B. Cronin, M. Ge, X. Fang, T. Nilges, and C. Zhou, "Black Arsenic-Phosphorus: layered anisotropic infrared semiconductors with highly tunable compositions and properties," Adv. Mater. **27**(30), 4423–4429 (2015).
19. M. Long, A. Gao, P. Wang, H. Xia, C. Ott, C. Pan, Y. Fu, E. Liu, X. Chen, W. Lu, T. Nilges, J. Xu, X. Wang, W. Hu, and F. Miao, "Room temperature high-detectivity mid-infrared photodetectors based on black arsenic phosphorus," Sci. Adv. **3**(6), e1700589 (2017).
20. X. Wang and S. Lan, "Optical properties of black phosphorus," Adv. Opt. Photonics **8**(4), 618–655 (2016).
21. S. Yuan, C. Shen, B. Deng, X. Chen, Q. Guo, Y. Ma, A. Abbas, B. Liu, R. Haiges, C. Ott, T. Nilges, K. Watanabe, T. Taniguchi, O. Sinai, D. Naveh, C. Zhou, and F. Xia, "Air-stable room-temperature mid-infrared photodetectors based on hBN/black arsenic phosphorus/hBN heterostructures," Nano Lett. **18**(5), 3172–3179 (2018).
22. V. Ryzhii, M. Ryzhii, D. Svintsov. V. Leiman, V. Mitin, M. S. Shur, and T. Otsuji, "Infrared photodetectors based on graphene van der Waals heterostructures," Infrared Phys. Technol. **84**, 72–81 (2017).

Optics EXPRESS

23. V. Ryzhii, M. Ryzhii, V. Leiman, V. Mitin, M. S. Shur, and T. Otsuji, "Effect of doping on the characteristics of infrared photodetectors based on van der Waals heterostructures with multiple graphene layers," J. Appl. Phys. **122**(5), 054505 (2017).
24. V. Ryzhii, M. Ryzhii, D. Svintsov, V. Leiman, V. Mitin, M. S. Shur, and T. Otsuji, "Nonlinear response of infrared photodetectors based on van der Waals heterostructures with graphene layers," Opt. Express **25**(5), 5536–5549 (2017).
25. V. Ryzhii, T. Otsuji, V. E. Karasik, M. Ryzhii, V. G. Leiman, V. Mitin, and M. S. Shur, "Comparison of intersubband quantum-well and interband graphene-layer infrared photodetectors," IEEE J. Quantum Electron. **54**(2), 1–8 (2018).
26. G. Gong, H. Zhang, W. Wang, L. Colombo, R. M. Wallace, and K. Cho, "Band alignment of two-dimensional transition metal dichalcogenides: Application in tunnel field effect transistors," Appl. Phys. Lett. **103**(5), 053513 (2013).
27. Y. Cai, G. Zhang, and Y.-W. Zhang, "Layer-dependent band alignment and work function of few-layer phosphorene," Sci. Rep. **4**(1), 6677 (2015).
28. Yu Li, Yi Shi, and X. Wang, "Electrically tunable optical properties of few-layer black arsenic phosphorus," Nanotechnology **29**(48), 484001 (2018).
29. Y. Chen, C. Chen, R. Kealhofer, H. Liu, Z. Yuan, L. Jiang, J. Suh, J. Park, C. Ko, H. S. Choe, J. Avila, M. Zhong, Z. Wei, J. Li, S. Li, H. Gao, Y. Liu, J. Analytis, Q. Xia, M. C. Asensio, and J. Wu, "Black Arsenic: a layered semiconductor with extreme in-plane anisotropy," Adv. Mater. (Weinheim, Ger.) **30**(30), 1800754 (2018).
30. V. Ryzhii, A. Satou, T. Otsuji, M. Ryzhii, V. Mitin, and M. S. Shur, "Graphene vertical hot-electron terahertz detectors," J. Appl. Phys. **116**(11), 114504 (2014).
31. M. Ryzhii, V. Ryzhii, V. Mitin, M. S. Shur, and T. Otsuji, "Vertical hot-electron terahertz detectors based on black-$As_{1-x}P_x$/graphene/black-$As_{1-y}P_y$ heterostructures," Sens. Mater. **31**(7), 2271–2279 (2019).
32. W. C. Tan, Y. Cai, R. J. Ng, L. Huang, X. Feng, G. Zhang, Y.-W. Zhang, C. A. Nijhuis, X. Liu, and K.-W. Ang, "Few-layer black phosphorus carbide field-effect transistor via carbon doping," Adv. Mater. (Weinheim, Ger.) **29**(24), 1700503 (2017).
33. W. C. Tan, L. H. Huang, E. J. Ng, L. Wang, D. Md. Naruddin Hasan, T. J. Duffin, K. S Kumar, C. A. Nijhuism, C. Lee, and K.-W. Ang, "A black phosphorus carbide infrared phototransistor," Adv. Mater. (Weinheim, Ger.) **30**(6), 1705039 (2018).
34. M. Ershov, V. Ryzhii, and C. Hamaguchi, "Contact and distributed effects in quantum well infrared photodetectors," Appl. Phys. Lett. **67**(21), 3147–3149 (1995).
35. L. Thibaudeau, P. Bois, and J. Y. Dubos, "A self - consistent model for quantum well infrared photodetectors," J. Appl. Phys. (Melville, NY, U. S.) **79**(1), 446–454 (1996).
36. V. Ryzhii, T. Otsuji, M. Ryzhii, V. Ya. Aleshkin, A. A. Dubinov, V. Mitin, and M. S. Shur, "Vertical electron transport in van der Waals heterostructures with graphene layers," J. Appl. Phys. **117**(15), 154504 (2015).
37. H. C. Liu, "Photoconductive gain mechanism of quantum well intersubband infrared detectors," Appl. Phys. Lett. **60**(12), 1507–1509 (1992).
38. E. Rosencher, B. Vinter, F. Luc, L. Thibaudeu, P. Bois, and J. Nagle, "Emission and capture of electrons in multiquantum-well structures," IEEE J. Quantum Electron. **30**(12), 2875–2888 (1994).
39. V. Ryzhii, "Characteristics of quantum-well infrared photodetectors," J. Appl. Phys. **81**(9), 6442–6448 (1997).
40. V. Ya. Aleshkin, A. A. Dubinov, M. Ryzhii, V. Ryzhii, and T. Otsuji, "Electron capture in van der Waals graphene based heterostructures with WS_2 barrier layers," J. Phys. Soc. Jpn. **84**(9), 094703 (2015).
41. V. Ryzhii, I. Khmyrova, M. Ryzhii, R. Suris, and C. Hamaguchi, "Phenomenological theory of electric-field domains induced by infrared radiation in multiple quantum well structures," Phys. Rev. B **62**(11), 7268–7274 (2000).
42. V. Ryzhii and R. A. Suris, "Nonlocal hot-electron transport and capture model for multiple quantum well structures excited by infrared radiation," Jpn. J. Appl. Phys. **40**(Part 1, No. 2A), 513–517 (2001).
43. I. S. Gradstein and I. M. Ryzhik, "Table of Integrals, Series, and Products," (Academic, 1980).
44. R. B. Dingle, "Fermi-Dirac integrals," Appl. Sci. Res. **6**(1), 225–239 (1957).
45. S. Luryi, "Quantum capacitance devices," Appl. Phys. Lett. **52**(6), 501–503 (1988).
46. H. Liu, Y. Du, Y. Deng, and P. D. Ye, "Semiconducting black phosphorus: synthesis, transport properties and electronic applications," Chem. Soc. Rev. **44**(9), 2732–2743 (2015).
47. I. Grave and A. Yariv, "Fundamental limits in quantum well intersubband detection," in *Intersubband Transitions in Quantum Wells*, E. Rosencher, B. Vinter, and B. Levine, eds. (Plenum Press, 1992).
48. V. Ryzhii, I. Khmyrova, V. Mitin, M. Stroscio, and M. Willander, "On the detectivity of quantum-dot infrared photodetectors," Appl. Phys. Lett. **78**(22), 3523–3525 (2001).
49. V. Ryzhii, M. Ryzhii, and V. Mitin, "Comparison of dark current, responsivity and detectivity in different intersubband infrared photodetectors," Semicond. Sci. Technol. **19**(1), 8–16 (2004).
50. A. Rogalski, "Semiconductor detectors and focal plane arrays for far-infrared imaging," Opto-Electron. Rev. **21**(4), 404–426 (2013).
51. S. D. Gunapala, S. V. Bandara, J. K. Liu, J. M. Mumolo, S. B. Rafol, D. Z. Ting, A. Soibel, and C. Hill, "Quantum well infrared photodetector technology and applications," IEEE J. Sel. Top. Quantum Electron. **20**(6), 154–165 (2014).

Optics EXPRESS

52. H. C. Liu, G. E. Jenkins, E. R. Brown, K. A. McIntosh, K. B. Nichols, and M. J. Manfra, "Optical heterodyne detection and microwave rectification up to 26 GHz using quantum well infrared photodetectors," IEEE Electron Device Lett. **16**(6), 253–255 (1995).
53. H. C. Liu, J. Li, E. R. Brown, K. A. McIntosh, K. B. Nichols, and M. J. Manfra, "Quantum well intersubband heterodyne infrared detection up to 82 GHz," Appl. Phys. Lett. **67**(11), 1594–1596 (1995).
54. D. Palaferri, Y. Todorov, A. Bigioli, A. Mottaghizadeh, D. Gacemi, A. Calabrese, A. Vasanelli, L. Li, A. G. Davies, E. H. Linfield, F. Kapsalidis, M. Beck, J. Faist, and C. Sirtori, "Room-temperature nine-μm-wavelength photodetectors and GHz-frequency heterodyne receivers," Nature **556**(7699), 85–88 (2018).
55. K. K. Choi, S. C. Allen, J. G. Sun, Y. Wei, K. A. Olver, and R. X. Fu, "Resonant structures for infrared detection," Appl. Opt. **56**(3), B26–B36 (2017).
56. S. Kalchmair, R. Gansch, S. I. Ahn, A. M. Andrews, H. Detz, T. Zederbauer, E. Mujagic, P. Reininger, G. Lasser, W. Schrenk, and G. Strasser, "Detectivity enhancement in quantum well infrared photodetectors utilizing a photonic crystal slab resonator," Opt. Express **20**(5), 5622–5628 (2012).
57. V. Ryzhii, "The theory of quantum-dot infrared phototransistors," Semicond. Sci. Technol. **11**(5), 759–765 (1996).
58. S. Chakrabarti, A. D. Stiff-Roberts, X. H. Su, P. Bhattacharya, G. Ariyawansa, and A. G. U. Perera, "High-performance mid-infrared quantum dot infrared photodetectors," J. Phys. D: Appl. Phys. **38**(13), 2135–2141 (2005).
59. A. V. Barve, J. Montaya, Y. Sharma, T. Rotter, J. Shao, W.-Y. Jang, S. Meesala, S. J. Lee, and S. Krishna, "High temperature operation of quantum dots-in-a-well infrared photodetectors," Infrared Phys. Technol. **54**(3), 215–219 (2011).
60. B. Paulillo, S. Pirotta, H. Nong, P. Crozat, S. Guilet, G. Xu, S. Dhillon, L. H. Li, A. G. Davies, E. H. Linfield, and R. olombelli, "Ultrafast terahertz detectors based on three-dimensional meta-atoms," Optica **4**(12), 1451–1456 (2017).
61. V. Ryzhii, I. Khmyrova, and M. Ryzhii, "Impact of transit-time and capture effects on high-frequency performance of multiple quantum-well infrared photodetectors," IEEE Trans. Electron Devices **45**(1), 293–298 (1998).
62. V. Ryzhii, "High-frequency performance of single quantum well infrared photodetectors at high power densities," IEEE Trans. Electron Devices **45**(8), 1797–1803 (1998).